ACS OMEGA

Open Access

http://pubs.acs.org/journal/acsodf

Article

Biogenic Synthesis of Zinc Oxide Nanoparticles Mediated by the Extract of *Terminalia catappa* Fruit Pericarp and Its Multifaceted Applications

Published as part of the ACS Omega virtual special issue "Phytochemistry".

Cannon Antony Fernandes, Nameeta Jesudoss M, Aatika Nizam, Suresh Babu Naidu Krishna, and Vasantha Veerappa Lakshmaiah*

Cite This: *ACS Omega* 2023, 8, 39315−39328

Read Online

ACCESS | Metrics & More | Article Recommendations | Supporting Information

ABSTRACT: Zinc oxide nanoparticles (ZnO-NPs) were biosynthesized by using the pericarp aqueous extract from *Terminalia catappa* Linn. These NPs were characterized using various analytical techniques such as X-ray diffraction (XRD), Fourier transform infrared (FTIR) spectroscopy, ultraviolet (UV) spectroscopy, dynamic light scattering (DLS), and scanning electron microscopy (SEM), and XRD studies of the nanoparticles reported mean size as 12.58 nm nanocrystals with highest purity. Further SEM analysis emphasized the nanoparticles to be spherical in shape. The functional groups responsible for capping and stabilizing the NPs were identified with FTIR studies. DLS studies of the synthesized NPs reported ζ potential as −10.1 mV and exhibited stable colloidal solution. These characterized ZnO-NPs were evaluated for various biological applications such as antibacterial, antifungal, antioxidant, genotoxic, biocompatibility, and larvicidal studies. To explore its multidimensional application in the field of medicine. NPs reported a potential antimicrobial activity at a concentration of 200 μg/mL against bacterial strains in the decreasing order of *Streptococcus pyogenes* > *Streptococcus aureus* > *Streptococcus typhi* > *Streptococcus aeruginosa* and against the fungi *Candida albicans*. In vitro studies of RBC hemolysis with varying concentrations of NPs confirm their biocompatibility with IC_{50} value of 211.4 μg/mL. The synthesized NPs' DPPH free radical scavenging activity was examined to extend their antioxidant applications. The antiproliferation and genetic toxicity were studied with meristematic cells of *Allium cepa* reported with mitotic index (MI index) of 1.2% at the concentration of 1000 μg/mL. NPs exhibited excellent Larvicidal activity against *Culex quinquefasciatus* larvae with the highest mortality rate as 98% at 4 mg/L. Our findings elicit the therapeutic potentials of the synthesized zinc oxide NPs.

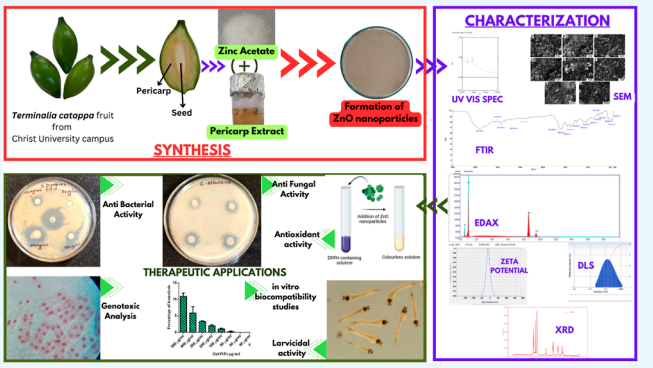

1. INTRODUCTION

Nanotechnology has attracted attention in recent times due to its multidimensional applications in revolutionizing the scientific world.[1] It has gained prime importance owing to the advantage of its surface area to volume ratio, which gives an edge while using it to work within the biological system. The potential applications of nanotechnology in therapeutics range from targeted drug delivery, efficient encapsulation, controlled/sustained drug release, imaging, enhancing diagnostics like the case of nano sensors, improving the efficacy and safety of implants, regenerative medicine, and in some cases, as the therapy itself.[2] Biosynthesized zinc oxide nanoparticles possess ample potentialities owing to their unique properties like small size and large surface area that enhances its reactivity, strong UV absorption, inherent antimicrobial properties that makes them useful in medical applications, being valuable in cancer therapy, and their photocatalytic properties that promotes them as an inevitable force in environmental remediation as well.[3,4]

In the current reported work, the biological potential and significance of the green synthesized zinc oxide nanoparticles from the pericarp of the fruit of *Terminalia catappa* Linn was evaluated. The plant has deep traditional roots in tropical India, and it is a commonly used ornamental plant in the subcontinent. It is a large tropical tree belonging to the family *Combretaceae*. Distribution of the tree is in the subtropical and

Received: July 6, 2023
Accepted: September 18, 2023
Published: October 9, 2023

tropical zones of the Indian and Pacific Oceans. The pericarp is traditionally used as an acrid, astringent, purgative, and aphrodisiac. It is also used to treat bronchitis, bowels, diabetes, leprosy, headache, and nausea.[5,6] The pericarp that is an agrowaste contains several secondary metabolites such as amino acids, alkaloids, phenolic compounds, and flavonoids (S1) that could mediate the reduction and can serve as capping for stable nanoparticle synthesis.[7] The aim of this work was to explore the potential of the pericarp extract in the formation and stabilization of ZnO nanoparticle synthesis as a sustainable and economical method of synthesis. The crystal structure and surface morphology were characterized using UV−visible spectroscopy, FTIR, zeta potential, XRD, dynamic light scattering, EDAX, and SEM images. The substantial characterization results prompted us to examine their biological potentials. Zinc oxide (ZnO) nanoparticles are biologically safe nanoparticles extensively used in various applications owing to their unique properties, such as antimicrobial, antioxidant, photooxidation, and photocatalysis. In order to test the antimicrobial activity of the synthesized zinc oxide nanoparticle, the antibacterial activity of the synthesized zinc oxide nanoparticle was evaluated against human pathogens of medical interest such as *Staphylococcus aureus*, *Streptococcus pyogenes*, *Pseudomonas aeruginosa*, and *Salmonella enterica* subsp. enterica serovar Typhimurium.[8] The effective antifungal property was reported against *Candida albicans*. To highlight, *S. aureus* is known to cause skin infections majorly and sometimes even pneumonia, *S. pyogenes* cause major acute infections, *P. aeruginosa* can cause pneumonia, and *S. enterica* subsp. enterica serovar Typhimurium can cause enteric diseases. The test fungal species chosen was *C. albicans* since it is the most prevalent fungus found in the human body and an opportunistic pathogen.[9] These test microbial organisms were chosen since they are all human pathogenic bacteria and understanding the antimicrobial effects can pave the way as nano pharmacological agents.

In order to assess the larvicidal properties of the synthesized zinc oxide nanoparticles, larvae of *Culex quinquefasciatus* were used, as they are the vectors for major zoonotic diseases. Elucidating larvicidal properties of the synthesized zinc oxide nanoparticle would further pave the way toward developing strategies to circumvent these diseases. The genotoxic and antimitotic effect of the synthesized nanoparticle was evaluated against the *Allium cepa* root tip. The biocompatibility of the nanoparticle to the blood was evaluated.[10] Overall, this work is a novel approach for green synthesis of ZnO nanoparticles using pericarp extract of *T. catappa* and elucidates their significant application as therapeutic agent.

2. MATERIALS AND METHODS

2.1. Test Microorganisms Used. Gram-positive bacteria *S. aureus* subsp. Aureus (ATCC 6538P) and *S. pyogenes* (ATCC 19615), Gram-negative bacteria *P. aeruginosa* (ATCC 27853), and *S. enterica* subsp. enterica serovar Typhimurium (ATCC 14028TM) was used as test bacterial strain, and *C. albicans* (ATCC 90028TM) was used as test fungal strain for evaluating the antimicrobial activity of synthesized ZnO NPs.

2.2. Chemicals Used. Nutrient Broth (HiMedia Laboratories), Nutrient Agar (HiMedia Laboratories), Potato dextrose broth (HiMedia Laboratories), zinc acetate dihydrate [$Zn(CH_3COO)_2{\cdot}2H_2O$], sodium hydroxide (NaOH), azithromycin (15 mg/mL), fluconazole (25 mg/mL), DPPH solution (0.1 mM in methanol) from Sigma-Aldrich, Carnoy's Fixative II, 70% ethanol, 1%SDS (Thermo Fisher Scientific), and 1× PBS (Thermo Fisher Scientific).

2.3. Collection and Preparation of Aqueous Extract of *T. catappa* Pericarp. The fresh fruits of *T. catappa* were collected from the campus of Christ (Deemed to be University) situated at Hosur road, Bangalore, India (12.939233°N, 77.550996°E). The plant leaves were used to make the herbarium and deposited with voucher number CULS_TC_002 at the Department of life sciences, Christ (Deemed to be university), Hosur road, Bangalore, for reference (Figure 1).

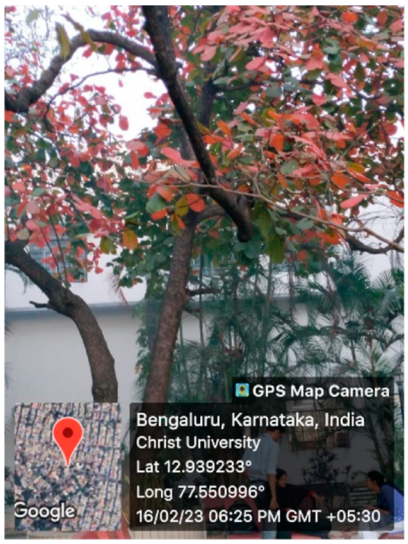

Figure 1. *Terminalia catappa* tree at CHRIST University, Bengaluru.

The fresh fruits of *T. catappa* were subjected to thorough washing with deionized water in an effort to remove the dust and the organic impurities. The synthesis of ZnO nanoparticles was performed as per Aminuzzaman et al., 2018.[11] Accordingly, 8 g of the fruit pericarp was taken and chopped into fine pieces. 100 mL of deionized water was added to the finely chopped pericarp pieces and was boiled at 70−80 °C in a water bath for 30 min until a golden yellow solution was obtained. The extract was then cooled until it attained the room temperature. Further, the extract was filtered using Whatman no. 1 paper. The filtration was repeated twice and the filtrate was stored in a 100 mL glass beaker. This filtrate (referred as pericarp extract) was then used further for the synthesis of ZnO nanoparticles (S2).

2.4. Synthesis of ZnO Nanoparticles. 50 mL of the pericarp extract prepared was boiled to the temperature range of 70−80 °C for about 10 min. Boiling was done to ensure increased reaction rates, enhanced solubility to facilitate homogeneous reaction, to trigger the decomposition of precursors, and to aid in improved nucleation and growth toward desired shape/size of NPs.[12] Four gram portion of zinc acetate dihydrate [$Zn\ (CH_3COO)_2{\cdot}2H_20$] was added to the boiling pericarp extract. Upon addition, a bright yellow-colored solution was formed on constant mixing in the magnetic stirrer. The pH was adjusted to alkaline range (pH 10) using 1 M NaOH. As the reaction progressed, the color changed and it was heated continuously to the point until a pale yellow (cream) precipitate was obtained. The precipitate was then washed multiple times using deionized water and was centrifuged at 5000 rpm for 10 min, followed by ethanol

https://doi.org/10.1021/acsomega.3c04857
ACS Omega 2023, 8, 39315−39328

wash at 5000 rpm for 5 min. The pellet obtained was dried at 60 °C in the hot air oven. The powder was then scrapped and stored in airtight vials for further characterization and biological studies.

2.5. Physico-Chemical Characterization of the Synthesized ZnO Nanoparticles. The ZnO nanoparticles synthesized were subjected to a series of characterization techniques. UV−vis Spectrophotometer (PerkinElmer, Lambda 30) was used to confirm the synthesis and to determine the optical density and energy gap of the synthesized ZnO nanoparticles. X-ray diffraction (XRD) study was performed with Miniflex 300/600 (Rigaku SmartLab, Tokyo, Japan), and Scherrer's formula was used to report the particle size of the nanoparticle. The dynamic light scattering (DLS) analysis was used to analyze the particle size distribution range of the synthesized ZnO nanoparticles. Morphological features of the biosynthesized ZnO nanoparticles were analyzed using a scanning electron microscope at 30 kV acceleration voltage. The elemental analysis of the ZnO nanoparticles was done through energy dispersive spectroscopy (EDS) in conjunction with the SEM analysis. The absorbance spectrum of ZnO nanoparticles was investigated by FT-IR in the 4000 to 400 cm^{-1} spectral range to identify the functional groups. The zeta potential measurement was to determine the net surface charge of the ZnO nanoparticles, which gives insight into their colloidal stability in suspension.

2.6. Evaluation of the Green Synthesized Nanoparticles for Biological Activities. *2.6.1. Antimicrobial Activity of ZnO Nanoparticles. 2.6.1.1. Estimation of Minimum Bactericidal Concentration (MBC) Using Kirby Bauer Test.* The in vitro antimicrobial activity of ZnO nanoparticles was evaluated by Disk diffusion method as per Clinical and Laboratory Standards Institute (CLSI) protocols.[12−14] 100 μL portion of mid log phase culture of bacteria *S. aureus* subsp. Aureus (ATCC 6538P), *S. pyogenes* (ATCC 19615), *P. aeruginosa* (ATCC 27853), *S. enterica* subsp. enterica serovar Typhimurium (ATCC 14028), and fungi *C. albicans* were spread plated on Mueller Hinton agar and potato dextrose agar, respectively. Sterile Whattman paper disc of 6 mm diameter was loaded with ZnO nanoparticles (50−200 μg/mL) and placed on the inoculated media. The bacterial cultures were incubated for 24 h at 37 °C, and the fungal cultures were incubated for 48 h incubation at 27 °C. The zones of inhibition in each case were observed and were measured in millimeters using an antibiotic zone scale (Hi media). Discs containing azithromycin (15 μg/mL) and fluconazole (25 μg/mL) were used as standard antibacterial and antifungal drugs, respectively.

2.6.1.2. Estimation of Minimum Inhibitory Concentration (MIC). The antimicrobial activity of biosynthesized ZnO nanoparticles was evaluated using the macro-dilution broth method, which is a commonly used antimicrobial technique for determining the minimum inhibitory concentration (MIC) of compounds. This technique was carried out in accordance with CLSI guidelines.[14] Concisely, mid log phase culture of bacterium *S. aureus* subsp. Aureus (ATCC 6538P), *S. pyogenes* (ATCC 19615), *P. aeruginosa* (ATCC 27853), *S. enterica* subsp. enterica serovar Typhimurium (ATCC 14028), and fungi *C. albicans* were diluted in Mueller Hinton broth and potato dextrose broth, respectively. The microbial inoculum load was adjusted to a 0.5 McFarland scale and then incubated. The nanoparticles of various concentrations (10−200 μg/mL) were supplemented into the inoculated medium. The bacterial cultures were incubated at 37 °C for 24 h, while the fungal culture was maintained at 27 °C for 24 h on a shaker incubator. The MIC values of the synthesized ZnO nanoparticles were compared with the standard antibiotics (Azithromycin and flucanazole) at the concentration of 1−10 g/mL. The experiments were performed in triplicates and the data obtained were expressed as mean ± standard deviation (SD).

2.6.2. Antioxidant Activity of Biosynthesized ZnO Nanoparticles. The antioxidant activity of the biosynthesized ZnO nanoparticles was determined using DPPH (1,1-diphenyl-2-picrylhydrazyl (DPPH) free radical scavenging activity.[15] Different concentrations of synthesized ZnO nanoparticles (20 to 100 μg/mL) were added to 2 mL of DPPH solution (0.1 mM in methanol). The reaction mixture was vortexed and incubated in the dark at room temperature for 30 min. Ascorbic acid was used as the standard. After the incubation, the absorbance was recorded at 517 nm.

The percentage of the DPPH radical scavenged was calculated as follows:

$$\text{scavenging effect percentage} = \frac{\text{control absorbance} - \text{sample absorbance}}{\text{control absorbance}} \times 100 \quad (1)$$

2.6.3. Genotoxicity Study of ZnO Nanoparticles Using A. cepa. The study was performed to investigate the genotoxic potential of the biosynthesized ZnO nanoparticles. The *A. cepa* root tips were used in this study.[16] Onion bulbs were grown in glass containers with sterile distilled water. When the root length reached 2 to 3 cm, they were transferred onto beakers containing ZnO nanoparticle solution (0.05−5 mg mL^{-1}). The root tips were then incubated for 48 h at room temperature. After incubation, the root tips were cut and fixed in Carnoy's Fixative II (for 24 h) and further transferred to 70% ethanol for storage.

The temporary squash preparation of the root tips was prepared using Acetocarmine staining, and the cells were observed for cell division stages under the microscope. The root tips grown in sterile distilled water served as control[16,17] against the root tips exposed to the ZnO nanoparticles. The mitotic index of the biosynthesized nanoparticle was calculated using the formula 2 mentioned.[18]

$$\text{Mitotic index} = \frac{\text{number of dividing cells}}{\text{total number of cells}} \times 100 \quad (2)$$

2.6.4. In Vitro Biocompatibility of ZnO Nanoparticles. In order to validate the biocompatibility of ZnO nanoparticles, a hemolytic assay was performed by using human red blood cells obtained from a healthy donor. In this assay, the percentage of hemolysis was noted against varying concentrations of ZnO nanoparticles (10−500 μg/mL). The positive and negative controls for the assay were 1% SDS and 1× PBS, respectively. Hemolysis of the blood RBC against the ZnO nanoparticles was measured at 540 nm by using a spectrophotometer. The concentration of released hemoglobin through RBC lysis was recorded. Further, the percentage of hemolysis was calculated using the formula 3 given below[19]

$$\%\ \text{hemolysis} = \frac{\text{test OD}}{\text{control OD}} \times 100 - \text{negative control OD} \quad (3)$$

https://doi.org/10.1021/acsomega.3c04857
ACS Omega 2023, 8, 39315−39328

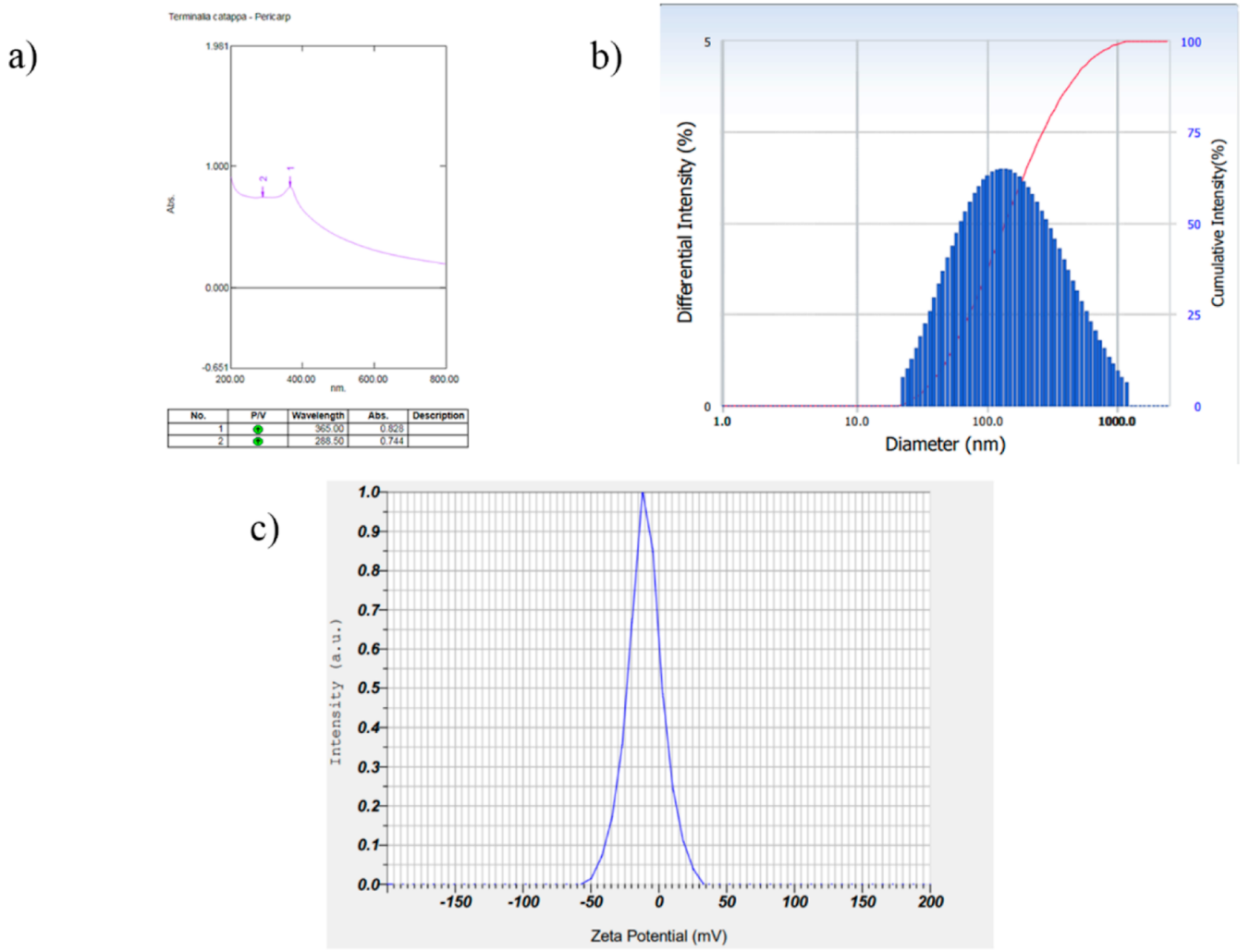

Figure 2. (a) UV−visible spectra for phyto-fabricated ZnO nanoparticles from *T. catappa* pericarp extract, (b) particle size distribution of green synthesized ZnO nanoparticles by intensity through DLS, and (c) zeta potential results of green synthesized ZnO nanoparticles from the pericarp extract of *T. catappa*.

2.6.5. Toxicity Effect of Nanoparticles on C. quinquefasciatus Larvae. *C. quinquefasciatus* larvae (fourth instar) were collected from the stagnant water of the Xavier Research Foundation, Palayamkottai campus (8.718775675142657N, 77.74043761672226E). They were reared in the laboratory following the standard methods.[20]

The larvicidal activity was monitored as per the standard protocol recommended.[21] The toxicity of the biosynthesized ZnO nanoparticles was analyzed in the cohort containing 20 mosquito larvae (*C. quinquefasciatus*). A comparative larvicidal activity was analyzed between the commercially obtained pure zinc oxide (25−3.12 mg/L) and the synthesized ZnO nanoparticles (4 to 0.5 mg/L). The number of dead larvae in the cohort after 24 h of exposure was recorded. Percentage of the mortality was calculated using the average obtained from the five replicates. The percentage mortality was calculated using formula 4 and the corrected percentage mortality data using standard formula 5 listed.[22]

$$\text{Percentage of mortality} = \frac{\text{number of dead larvae}}{\text{total number of larvae}} \times 100 \quad (4)$$

$$\begin{aligned}\text{corrected percentage of mortality} = [&(\text{percentage of mortality intreatment} \\ &- \text{percentage of mortality in control}) \\ &/(100 - \text{percentage of mortality in control})] \times 100\end{aligned} \quad (5)$$

2.6.5.1. Data Analysis. The data were analyzed using version 21.0 of the IBM SPSS software package for the entire study (SPSS 2012). LC50 and LC 90 values were determined using probit analysis. LC50 denotes the lethal concentration of the biosynthesized nanoparticle required to kill 50% of the larvae used and LC 90 pertains to the lethal concentration that kills 90% of the total larvae exposed. The results obtained were analyzed for statistical significance at the significance level of $p < 0.05$.

3. RESULTS AND DISCUSSION

3.1. Physico Chemical Characterization of ZnO Nanoparticles. *3.1.1. UV−Visible Spectroscopy.* The phyto-fabricated ZnO nanoparticles were subjected to UV−vis spectroscopy in the range of 200−800 nm. The obtained UV−visible spectral data showed an absorption maximum at

https://doi.org/10.1021/acsomega.3c04857
ACS Omega 2023, 8, 39315−39328

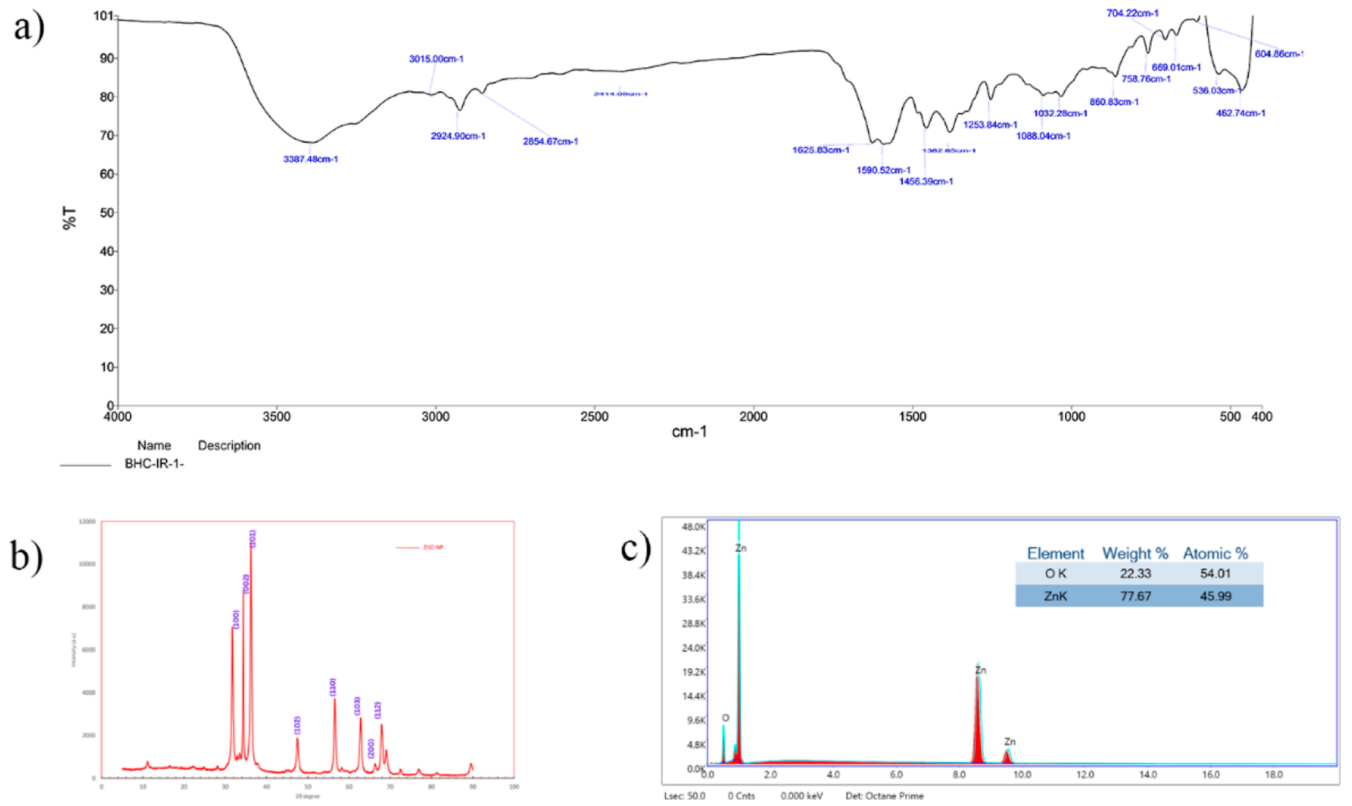

Figure 3. (a) FT-IR spectrum for biosynthesized zinc oxide nanoparticles, (b) XRD patterns of green synthesized ZnO nanoparticles from the pericarp of *T. catappa*, and (c) EDX spectra of zinc oxide nanoparticle synthesized from *T. catappa* pericarp.

365 nm that was the characteristic peak absorbance value for ZnO nanoparticles with an energy band gap of 3.403 eV, which was in accordance with the earlier reported works (Figure 2a). The literature suggests that the absorption peak maxima for ZnO nanoparticles was in the range of 280 to 400 nm and 3.2 to 3.5 eV.[23]

3.1.2. Dynamic Light Scattering. The Debye−Scherrer's equation is limited to spherical and semi spherical nanoparticles only.[24] To overcome the limitation and to measure the size without any constraints over the size and shape, dynamic light scattering (DLS) is used. The average hydrodynamic diameter (Dh) of ZnO nanoparticles was found to be 116.6 nm, which is larger than the sizes obtained from the SEM measurements. The larger size can be attributed to aggregation of NPs and hydrodynamical shell.[25] The polydispersity index was found to be 0.325 and the Diffusion Const. (D) was 4.219e−008 (cm^2/s) (Figure 2b).

3.1.3. Zeta Potential (ζ Potential). The size distribution and ζ-potential of the biosynthesized ZnO-NPs were investigated by using the dynamic light scattering (DLS) technique. The ζ-potential defines the colloidal stability and is a typical measurement of the surface charge of a particle. Aqueous suspensions that exhibit 15 mV are generalized as stable colloids.[25] In the study, the ζ-potential of the ZnO nanoparticles in distilled water (DW) was measured as −10.1 mV, and this can thus be considered relatively anionic (Figure 2c). The ζ potential measurements, thus, verify and support the dispersion capacity of the greenly synthesized ZnO nanoparticles. The negative surface charge clearly indicates that the capping molecules from pericarp extracts were negatively charged and are responsible for steadiness of the zinc oxide nanoparticles by alleviating the aggregation potential of the particles.[26] Different functional groups (carbohydrates, polysaccharides, pectin, and so forth) present in fruit extract adsorbed on the surface of the nanoparticles may affect its ζ-potential. There is a close relationship between these metabolites absorbed on the surface of ZnO nanoparticles and ζ-potential.

3.1.4. Fourier Transform Infrared Spectroscopy. The FT-IR analysis was done in the range of 400−4000 cm^{-1} to report the constituent functional groups found in the synthesized ZnO nanoparticles, as shown in Figure 3a. The reference to identify the absorption peaks were with respect to the standardized IR spectrum table.[27] In the case of the biosynthesized ZnO nanoparticles from the pericarp extract of *T. catappa* Linn., the intense absorption peak at 3387.48 cm^{-1} signifies the O−H stretch, which is a functional group of alcohol. Peaks obtained at 3015 cm^{-1} confirms the O−H stretching of carboxylic acid whereas the peaks at 2924.9 and 2854.67 cm^{-1} indicate the presence of C−H stretch. The bands at 1625.83 and 1590.52 cm^{-1} are C═C stretch of alkene and cyclic alkenes, respectively. Medium peaks at 1456.39 and 1382.65 cm^{-1} illustrate the C−H bending of the alkanes. The S═O stretch of sulfate was related to the peak found at 1382.65 cm^{-1}. The absorption at 1253.84 cm^{-1} is due to the C−O stretch in the aromatic ester. Further, the C−N stretch of the amines was confirmed with the absorption peaks found at 1088 and 1032 cm^{-1}. This FT-IR spectrum analysis gives an overall view of the functional groups of the synthesized ZnO nanoparticles.[28]

3.1.5. X-ray Diffraction Analysis. The structural identification and composition analysis of the ZnO nanoparticles were identified by X-ray diffraction. The XRD patterns of synthesized ZnO nanoparticles by green synthesis is shown in

https://doi.org/10.1021/acsomega.3c04857
ACS Omega 2023, 8, 39315−39328

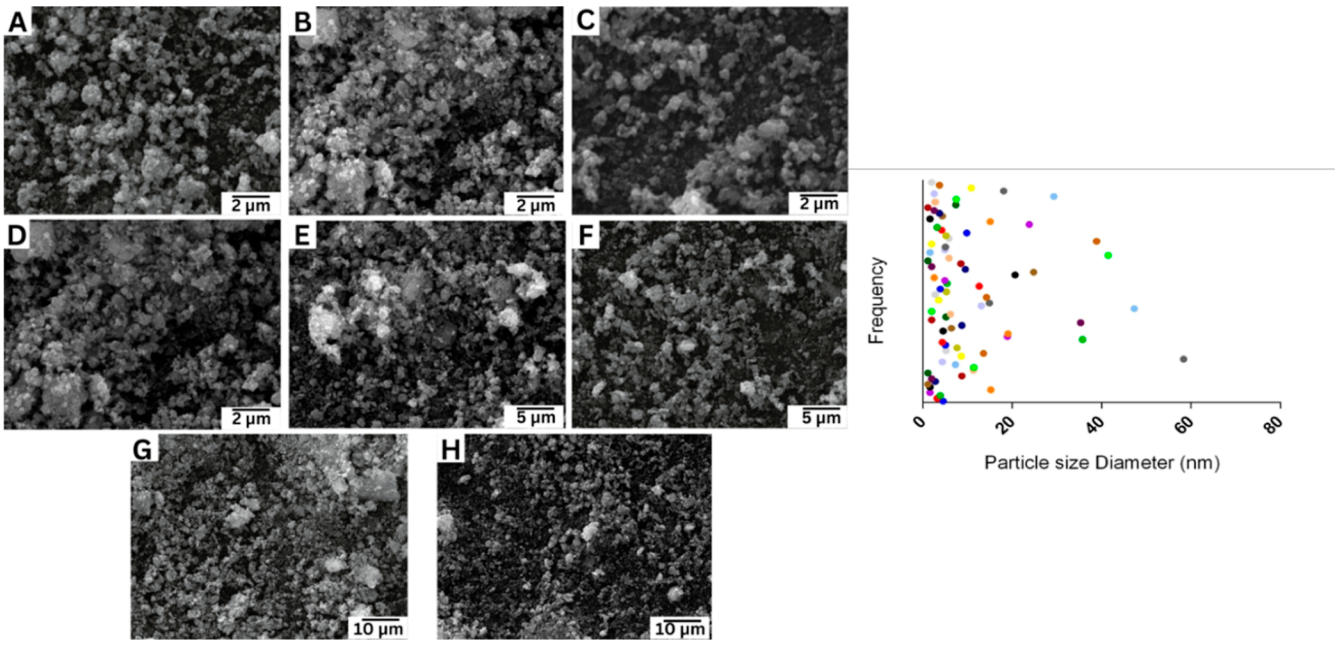

Figure 4. SEM analysis of green synthesized ZnO nanoparticles from *T. catappa* pericarp extract (magnification of A,B,C,D, 2 μm; E,F, 5 μm; G,H, 10 μm) and a scatter plot showing the distribution of particle size diameter through SEM analysis.

Figure 3b. It exhibited three strong diffraction peaks of 2θ (31.770, 34.404, 36.248°) associated with planes (100), (002), (101), and other peaks for (102), (110), (103), (200), and (112) planes. The pattern of the peaks obtained pertains to the pure ZnO with a hexagonal wurtzite-type structure.[29,30] The crystallographic parameters such as average crystalline size (D), microstrain, dislocation density, and specific surface area of Zn−Sn−Co−S were calculated from the different diffraction angle peak of the XRD pattern by using Scherer's equation, and the results are summarized in S3.

$$D_{hkl} = \frac{k\lambda}{\beta \cos \theta} \tag{6}$$

where D is crystallite size, k is constant shape factor with value 0.9, λ is the wavelength of X-ray radiation in nanometer, β is the full width at half-maximum (fwhm) in radian, and θ is the angle between incident and diffracted beams in degree. Here, using formula 6, we found that the D values of prepared NPs are between 44 and 59 nm and the evaluated values were calculated from the different angles shown in S3. The dislocation density was calculated for all prepared nanoparticle samples by using formula 7 and the evaluated values are shown in S3.

$$\delta = \frac{1}{D^2} \tag{7}$$

The dislocation density decreased with the increase in the angle, which may be attributed to the increase of the crystal structure. The micro strain value was analyzed using formula 8. The decrease in the microstrain was due to the increased angle as a result of difference in the dislocation density (δ), fwhm, and the crystallite size (D).

$$\text{Microstrain } (\varepsilon) = \frac{\beta \cos \theta}{4} \tag{8}$$

3.1.6. Energy Dispersive X-ray Composition Analysis. EDX analysis was carried out along with SEM to determine the surface elemental composition of the synthesized ZnO nanoparticles. The EDX spectra confirmed the presence of elements Zn and O in the nanoparticle.[24] This was validated by the presence of peaks that correspond to the optical absorption pertaining to the biosynthesized nanoparticle from the pericarp extract of *T. catappa*. Clear signals of Zn and O were observed in the spectra that confirmed the purity of the synthesized nanoparticle. The elemental mapping analysis revealed that the quantities of Zn and O were 77.67 and 22.33% when measured in weight percentage. The atomic percentage of Zn and O was analyzed to be 54.01 and 45.99%, respectively. The details of the EDX spectra of the synthesized nanoparticles are listed in Figure 3c. The data obtained reveal that the synthesized ZnO nanoparticles had good purity (77.67% of Zn and 22.33% of O) that is 4:1 ratio of Zn and O, respectively.

3.1.7. Scanning Electron Microscopy of ZnO Nanoparticles. The morphological analysis of ZnO nanoparticles synthesized from the pericarp extract of *T. catappa* was performed using SEM images. The micrographs revealed that the nanoparticles appeared as irregular spherical structures existing in a highly agglomerated form (Figure 4). The particle size ranged from 1 to 30 nm with higher frequency of the particles in the range of 1−20 nm (Figure 4) that were in agreement with earlier reports confirming green synthesized ZnO nanoparticles in the range 5−40 nm and in spherical shape.[31,32] The average diameter was analyzed to be 12.58 nm. The increase in size is possibly due to the overlapping of particles.

3.2. Evaluation of the Green Synthesized Nanoparticles for Biological Activities. *3.2.1. Antimicrobial Activity of ZnO Nanoparticles.* The antimicrobial activity of the ZnO NPs was tested against strains of bacteria and fungi. Their microbicidal activities were examined at different concentrations (50−200 μg) by disc diffusion method along with the positive control. To evaluate the antimicrobial activity of the biosynthesized ZnO NPs, the nanoparticle was tested against microbial strains using the disk diffusion method. The

https://doi.org/10.1021/acsomega.3c04857
ACS Omega 2023, 8, 39315−39328

list of test microorganisms used in this study were—*S. aureus*, *S. Pyogenes* (representatives of Gram-positive bacteria) and *S. typhi*, *P. aeruginosa* (representatives of Gram-negative bacteria). In the case of the fungus, *C. albicans* was used. The presence of an inhibition zone clearly indicated the antibacterial effect of ZnO nanoparticles. Similar to the observations in the earlier studies,[33] it was noticed here that with increase in the concentration of ZnO nanoparticles, greater was the inhibition of the growth. The diameter of the inhibition zone differed in accordance with the bacterium and the concentrations of ZnO nanoparticles as mentioned in the Table 1.

Table 1. Antimicrobial Activity of *T. catappa* Pericarp-Synthesized ZnO Nanoparticles

concentration (μg/mL)	zone of inhibition (ZOI) in mm				
	bacterial strains				fungal strain
	Gram-positive		Gram-negative		
	S. aureus	S. pyogenes	S. typhi	P. aeruginosa	C. albicans
50		9			6
100		12			8
150	8	15	7		9
200	9	19	8		12
azithromycin (15 μg/mL)	20	22	20	21	
fluconazole (25 μg/mL)					12

Macro-dilution broth method was used to evaluate the MIC for the produced ZnO NPs because the disc diffusion method had shown that they had antibacterial capabilities. Synthesized ZnO NPs displayed MIC values of 26.66 ± 4.71, 126.66 ± 4.71, and 140 ± 8.16 μg/mL against *S. pyogenes*, *S. aureus*, and *S. typhi*, respectively, as shown in Figure 5a. In the case of *P. aeruginosa*, the value was found to be >200 μg/mL. The MIC value of 23.33 ± 4.71 μg/mL was obtained for *C. albicans*. The results indicate that the synthesized ZnO nanoparticles can inhibit *S. pyogenes* at the lowest concentration followed by *S. aureus* and then *S. typhi*. The nanoparticles can also inhibit the growth of the fungal species *C. albicans* at a lower concentration. The initial results obtained indicate the prospects of using the synthesized nanoparticles as a promising approach to combat the undesirous bacterial and fungal growth. Further understanding of the mechanism that the nanoparticles adopt against the microorganisms can be used to develop therapeutic approaches against human pathogenic bacteria and fungi.

The standard antibacterial drug Azithromycin indicated MIC values of 2.0 ± 0.81, 3.67 ± 0.47, 5.0 ± 0.81, and 7.33 ± 0.47 mg/100 μL against *S. pyogenes*, *S. aureus*, *S. typhi*, and *P. aeruginosa*, respectively. In the case of antifungal activity, fluconazole as a standard indicated MIC of 2.67 ± 0.47 against *C. albicans*.

Reports of studies conducted earlier affirm the fact that the plant-mediated synthesis of zinc oxide nanoparticle possess better biological potential than the nanoparticles synthesized through chemical methods.[34] Our study shows that the synthesized zinc oxide nanoparticles have a high rate of inhibition against *S. pyogenes* and a considerable rate of growth inhibition against *S. aureus* (Figure 5b). The results are in line with the previously reported works concluding that the phyto-synthesized zinc oxide nanoparticles are effective against Gram-positive bacteria.[35−37] Despite that the zinc oxide nanoparticle exert increased antimicrobial activity against various strains, it is to note that the Gram-positive bacteria are more sensitive to the nanoparticles compared to Gram-negative bacteria.[38] It is to note here in this case as well that the synthesized zinc oxide nanoparticles had the least effect on the growth of Gram-negative bacteria—*Salmonella typhimurium* and *P. aeruginosa*. The resistance offered by Gram-negative bacteria can be explained with respect to their cell wall structure and composition. The cell wall of Gram-negative bacteria includes an additional membrane with lipopolysaccharide which provides an additional barrier which resists the action of the nanoparticle[39] (S4a).

The possible mechanisms by which the zinc oxide nanoparticles exhibit antimicrobial activity is explained in S4b. The primary reason is the induction of ROS (reactive oxygen species) that induces oxidative stress, disruption of the membrane, and further DNA damage, which causes death of the bacterium.[40] The next possible antibacterial mechanism is due to the release of Zn^{2+} ions that interacts with the cell membrane and disintegrates the integrity of the membrane causing death ultimately.[41] The third mechanism for increased antibacterial activity of the biosynthesized zinc oxide nanoparticle is through direct interaction between the nanoparticle and cell membrane through electrostatic forces arising due to the accumulation of the nanoparticle on the surface that disrupts the membrane and causes leakage of the cellular components. These are the possible explanation for the increased antibacterial efficacy of biosynthesized zinc oxide against microbes.[42]

The synthesized zinc oxide nanoparticle shows effective antifungal activity against *C. albicans*, the most important fungal pathogen that is a threat to human health.[43] This observation is in line with the earlier reported works on zinc oxide nanoparticles and *C. albicans* (Figure 5c). This is supposedly due to their physiochemical stability and the surface attraction properties that they find use in extensive biomedical applications. Hence, ZnO nanoparticles are recognized to be the safest nanoparticles by the FDA-USA (21CFR182.8991).[44] The studies reported earlier elucidate the following possible reasons for the zinc oxide nanoparticles to exhibit increased fungicidal properties against *C. albicans*. The prime possibility is due to the surface interaction of the zinc oxide nanoparticle with the fungal cell wall. FTIR analysis was used to point out the functional groups that were responsible for these interactions, which indicates the possible interaction of alcohol, amide, methyl, alkynes, and phosphate groups, present on the surface of the nanoparticle, with the yeast cell wall.[45] The above listed interactions lead to the accumulation of the nanoparticle on the cell membrane that further leads to membrane disruption.[46] It is also suggested that the exposure to zinc oxide nanoparticles alters the cell structure like—breakage of hyphae, pitting of the cell wall, invagination of the surface, and cell membrane rupture. These factors can be viewed as the possible reasons for the observed cytotoxicity (S4c).

3.2.2. Antioxidant Activity of Synthesized ZnO Nanoparticles. The synthesized ZnO nanoparticles depicted considerable DPPH free radical scavenging activity when compared with ascorbic acid (reference standard). The IC50 values were calculated to be 49.1 ± 0.73 μg/mL for ascorbic

https://doi.org/10.1021/acsomega.3c04857
ACS Omega 2023, 8, 39315−39328

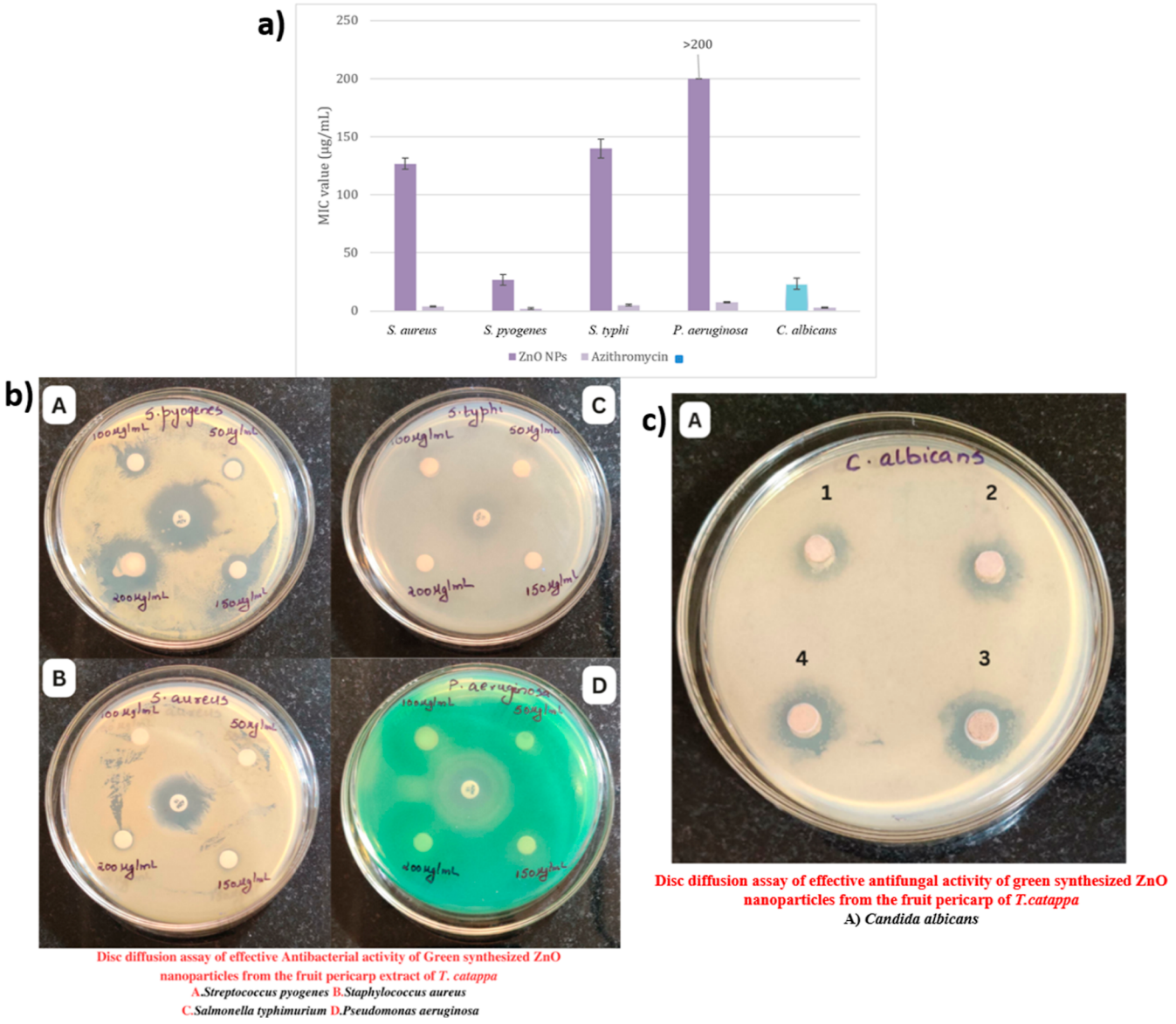

Figure 5. (a) Minimum inhibitory concentration (MIC) values of synthesized nanoparticles and standard antibiotics against test microbial strains by macrodilution broth method. Values are expressed as mean ± SD, $n = 3$ (b) antibacterial activity of synthesized ZnO nanoparticles from *T. catappa* pericarp (c) antifungal activity of synthesized ZnO nanoparticles from *T. catappa* pericarp.

acid and 41.03 ± 1.32 µg/mL for the synthesized ZnO nanoparticles (Figure 6). The antioxidant activity of the synthesized ZnO nanoparticles when compared with ascorbic acid showed a significant efficiency as that of the standard. Furthermore, there was an increase in its antioxidant activity with an increase in concentration. These findings were in agreement with the behavior of synthesized zinc oxide nanoparticles from the root extract of *Polygala tenuifolia*.[47] The scavenging activity is due to the transfer of electron from oxygen to nitrogen in DPHH that produces stable DPHH, which can be measured at 517 nm. This kind of strong antioxidant property of green synthesized nanoparticles is possibly due to the polyphenolic compounds that are present in the pericarp.[48,49]

3.2.3. Genotoxicity Study of ZnO Nanoparticles Using A. cepa. *A. cepa* serves as the bioindicator species for the genotoxicity analysis of the synthesized nanoparticles. Earlier works suggest that the phyto-fabricated zinc oxide nanoparticles were able to significantly affect cell division at the

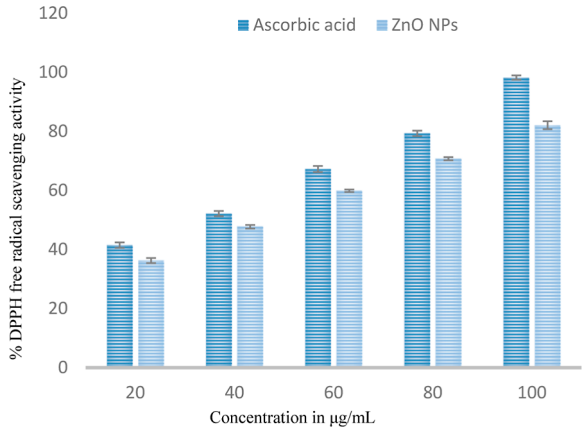

Figure 6. Results of antioxidant activity calculated using % DPPH free radical scavenging activity. Bars mean ± SD, $n = 3$.

https://doi.org/10.1021/acsomega.3c04857
ACS Omega 2023, 8, 39315−39328

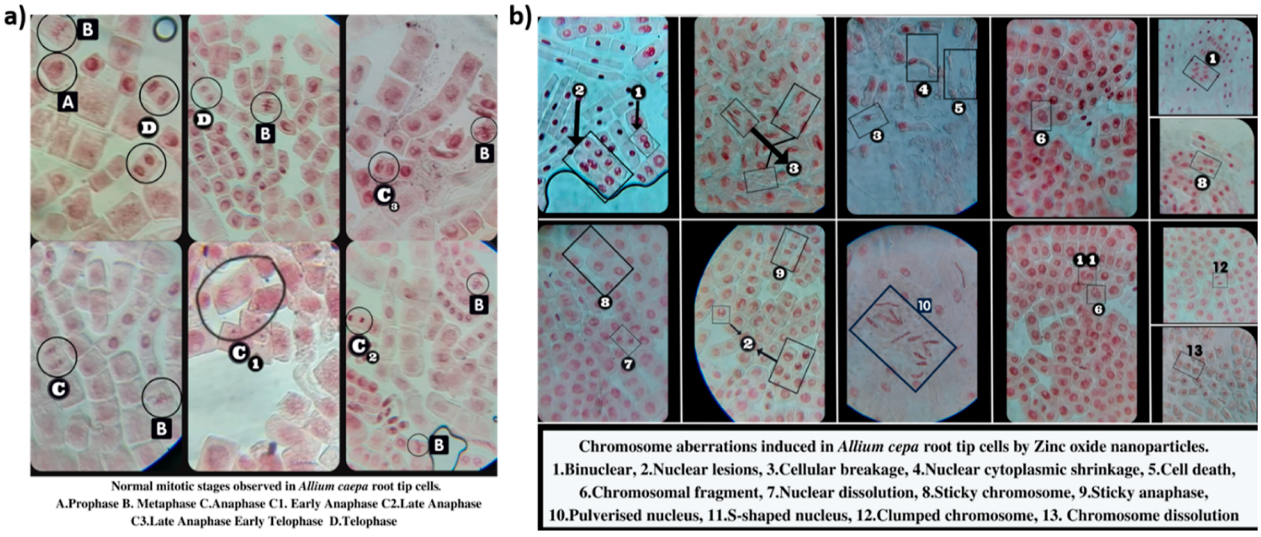

Figure 7. (a) Representative images of normal mitotic stages observed in *Allium cepa* root tips and (b) chromosomal aberrations observed in *Allium cepa* root tips by green-synthesized ZnO nanoparticles.

Table 2. Effects of ZnO Nanoparticles on Mitotic Cell Division and Mitotic Abnormalities in *A. cepa*

concentration of ZnO nanoparticles (μg mL^{-1})	no. of cells observed	no. of dividing cells	mitotic index (%)	chromosomal abnormality observed
0.00 (control)	250	165	66	no aberration
50.00	250	117	46.8	nuclear lesions, nuclear dissolution
100.00	250	90	36	binuclear, nuclear lesions, chromosomal dissolution, chromosomal fragment, clumped chromosome, S-shaped nucleus, binuclear
200.00	250	49	19.6	sticky chromosome, sticky anaphase, pulverised nucleus, nuclear cytoplasmic shrinkage, cellular breakage, binuclear
400.00	250	23	9.2	cell apoptosis
800.00	250	12	4.8	cell apoptosis
1000.00	250	3	1.2	cell apoptosis

mitotic stages in the onion root cells.[41] Hence, the antimitotic potentiality was analyzed and reported in *A. cepa* root tips.[50] The root tips exposed to ZnO nanoparticles showed chromosomal aberrations.[41] The inhibition of the cell division upon exposure to ZnO nanoparticles confirmed the genotoxic nature of the synthesized nanoparticles.[51] Some of the representative chromosomal aberrations observed were sticky or clumped chromosomes, chromosomes with spindle disturbance, fragmented chromosomes, micronucleus formation, nuclear lesions, early telophase, morphological alterations of the cell (pulverized nucleus, S-shaped nucleus), nuclear cytoplasmic shrinkage, and cellular breakage.[52−58]

Phytotoxicity assessments are vital since the plants occupy the first trophic level where the nanoparticles encounter the roots.[59] *A. cepa* treated with the synthesized ZnO nanoparticles from the aqueous pericarp extract of *T. catappa* Linn. Is believed to be a model for cytotoxicity assessment and visualizing oxidative DNA damage caused due to ROS production. The myriad of chromosomal damage can be well visualized in this experimental setup (Figure 7b). Previous studies report that the surface attachment, internalization, and biomolecular intervention of the nanoparticles on *A. cepa* root tip cells are believed to cause chromosomal aberrations.[60] This study highlights the cytotoxic and genotoxic effects of synthesized zinc oxide nanoparticles. The plausible mechanism for the dose-dependent cytotoxicity of the synthesized zinc oxide are due to the following reasons: internalization of the zinc oxide nanoparticles into the root cells, intracellular ROS production inducing mitochondrial and chromosomal damage (S5).[61]

The effect of ZnO nanoparticles on mitotic cell division and mitotic abnormalities in *A. cepa* root tips is shown in Table 2. There was an appreciable reduction in the mitotic index (%) with an increase in the concentration of ZnO nanoparticles. The minimum value of mitotic index was 1.2% in 1000 μg mL^{-1}. The concentrations such as 400, 800, and 1000 μg mL^{-1} showed maximum cell death. The control (Figure 7a) showed normal cell divisions, whereas the other concentrations such as 50, 100, and 200 μg mL^{-1} showed a higher number of aberrations (Figure 7b). The obtained results confirm that the ZnO nanoparticles showed higher genotoxic effects when the concentration was less than 1000 μg mL^{-1}.

Stickiness of chromosomes at the metaphase and anaphase was observed significantly in the nanoparticle-treated root tips. It indicated the polymerization effect of the synthesized ZnO nanoparticles on the nucleic acid of the chromosome and was a type of physical adhesion involving the proteinaceous matrix of the chromatin material. Observation of sticky bridges at anaphase recorded in higher doses could be attributed to chromosomal stickiness,[62] and chromosomal breakage and reunion.[63] Induction of chromosome bridges and breaks may lead to a loss of genetic material.

Binucleate cells, observed at higher ZnO nanoparticle concentrations, might be the result of the telophase suppression of cell wall formation. The micronuclei arose from the chromosomes that were lagging at the anatelophase

https://doi.org/10.1021/acsomega.3c04857
ACS Omega 2023, 8, 39315−39328

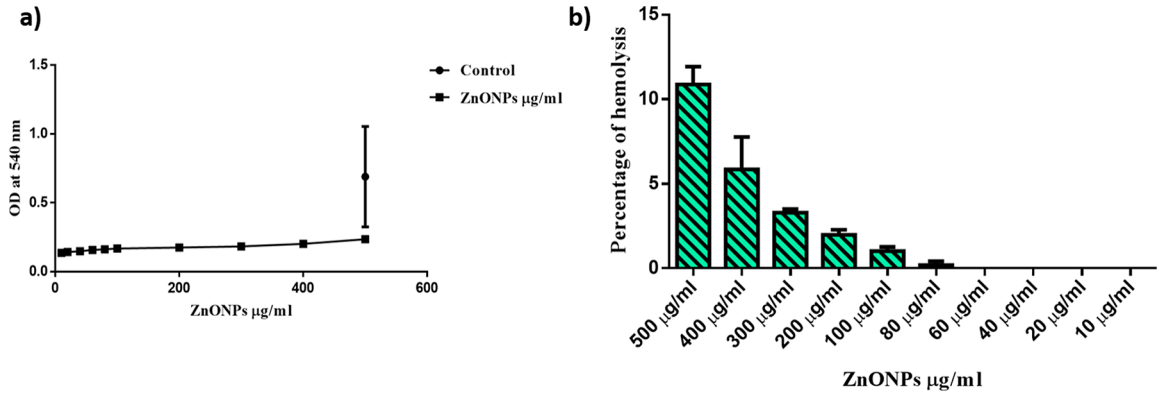

Figure 8. (a) Graph showing the mean OD values of the supernatant measured at 540 nm for varying concentrations of the nanoparticle and (b) percent hemolysis with varying concentrations of ZnO nanoparticles.

or from a chromosomal fragment. Micronuclei are thought to be a sign of mutagenicity of the inducers because they are true mutagenic segments that may result in the loss of genetic material.[64] It was claimed that ZnO nanoparticles had cytotoxic and genotoxic effects on the root tip cells of *A. cepa*, including lipid peroxidation, a decrease in the mitotic index, and an increase in the micronuclei and chromosomal aberration indices. Therefore, ZnO nanoparticles at higher concentrations could be mito-inhibitory.

3.2.4. In Vitro Biocompatibility of the ZnO Nanoparticles. Hemolysis of the RBCs is observed only if the sample has the ability to rupture the cells. The mechanism by which rupturing occurs is through the ROS produced by the biosynthesized zinc oxide nanoparticles, which causes oxidative stress and disturbed homeostasis, which ultimately leads to membrane damage and cell components leakage (S6).

Hemolytic effect of the biosynthesized ZnO nanoparticle is its ability to rupture the RBC, thereby causing the release of the hemoglobin. The concentration of the hemoglobin released can be measured by spectrophotometer by measuring absorbance at 540 nm (Figure 8a). Further the measured absorbance can be used to calculate the hemolysis percentage at different concentrations of the nanoparticles using the formula stated in the methods. The biocompatibility results are given in Table 3 and Figure 8b. According to the guidelines of the American Society for Testing Materials, the substances having >2% hemolysis are nonhemolytic, 2−5% are slightly hemolytic, and >5% are hemolytic. In this study, the ZnO nanoparticles showed increasing hemolysis with increasing concentration. The IC50 concentration for the sample was calculated as 211.4 μg/mL.

Table 3. % Hemolysis of Synthesized ZnO Nanoparticles

tested sample concentration (μg/mL)	mean value of hemolysis (%)
500	10.88534
400	5.853895
300	3.289792
200	1.983551
100	1.015965

3.2.5. Toxicity Effect of Nanoparticles on C. quinquefasciatus Larvae. Larvicidal activity of the synthesized ZnO nanoparticles was tested against larvae of *C. quinquefasciatus*, which is a vector for *Wuchereria bancrofti* that causes lymphatic filariasis. The ZnO nanoparticles shows an effective eradication of 98% at a maximum dosage of 4 mg/L. The LC_{50} and LC_{90} values of the synthesized nanoparticles toward the larvae were, 0.98 and 2.59 mg/L, respectively (Table 4 and Figure 9). The toxicity of nanoparticles on mosquito larvae can be attributed to their efficacy to penetrate through the insect's cuticle and, thereby, block the respiratory openings on the skin followed by suffocation and, ultimately, death.[65] Upon ZnO nanoparticles penetrating into the cuticle, it can induce morphological changes on the hemocytes upon exposure, thereby leading to deformations and decrease in their viability.[66,67] Additionally, the toxicity of ZnO nanoparticles to insects can be related to their ability to induce ROS and, thereby, cause the liberation of toxic ions inside the insect's cells.[66,68] Another larvicidal mechanism of ZnO nanoparticles can be related to their surface defects for a different texture.[69] These surface defects, especially at the corners and edges, can be abrasive and can damage the larva cell membrane. For instance, the needle and star shape of ZnO nanoparticles have more larvicidal efficacy through cutting the larval body, damaging the insect's midgut, and destroying the respiratory system (S7).[70,71]

4. CONCLUSIONS

To conclude, this work reports the synthesis of biologically significant ZnO nanoparticles by plant-mediated synthesis using the pericarp extract of *T. catappa*. The article highlights the characterization of the multifunctional ZnO nanoparticles obtained using the fruit pericarp extract of *T. catappa* Linn. by XRD, FTIR, DLS, EDX, and SEM analysis. The green synthesized nanoparticles were examined for various biological

Table 4. Larvicidal Activity of Synthesized ZnO Nanoparticles on *C. quinquefasciatus* Larvae

c	mortality	percent mortality (mg/L) ± SE	LC_{50} (mg/L)	UCL−LCL (mg/L)	LC_{90} (mg/L)	UCL−LCL (mg/L)	r^2	x^2 (df = 2)
4.0	19.6	98 ± 1.22	0.98	1.27−0.72	2.59	4.8−1.87	0.85	0.527
2.0	16.6	83 ± 1.22						
1.0	9.0	45 ± 2.23						
0.5	4.4	22 ± 1.22						

https://doi.org/10.1021/acsomega.3c04857
ACS Omega 2023, 8, 39315−39328

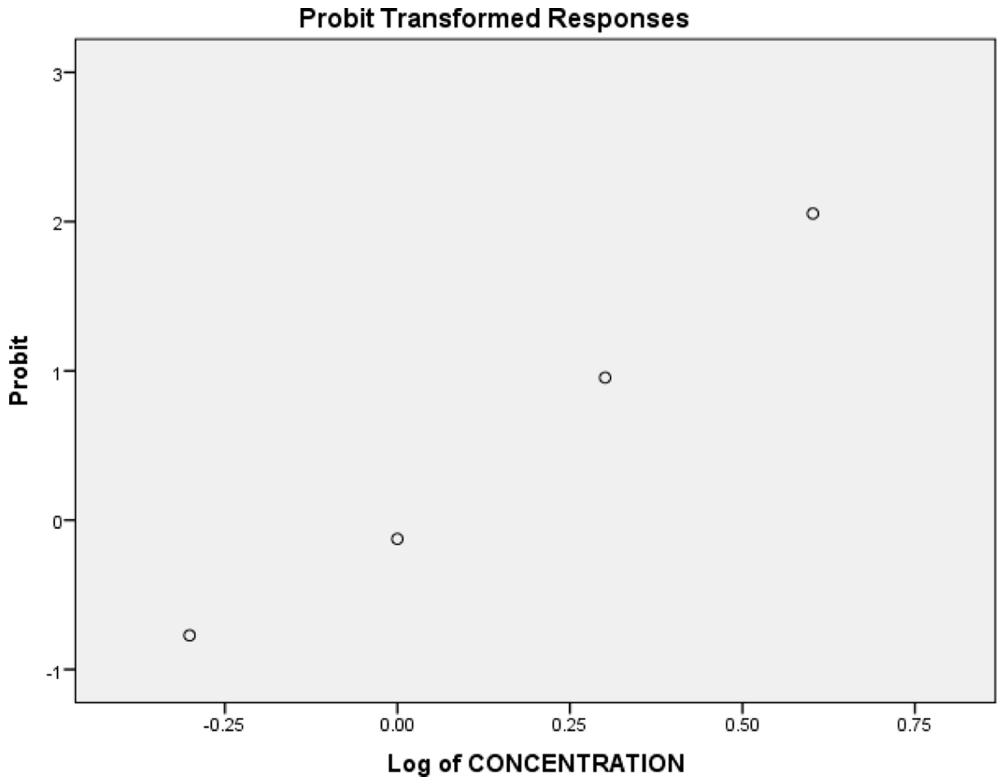

Figure 9. Scatter plot of probit analysis for the toxicity of the synthesized nanoparticles.

applications. The genotoxicity and cytotoxicity on the actively dividing cells emphasize their scope to be used against cancer cells as mitotic inhibitors. One of the challenges in the health sector is to address the multi drug resistant human pathogens. In this study, the nanoparticle was found to have successful capacity to inhibit potent human pathogens and, thus, emerging as a promising therapeutic agent against trivial bacterial and fungal infections. The antimicrobial studies exhibited a dose-dependent fashion as the zones of inhibition increased with increasing concentrations of ZnO nanoparticles. The synthesized ZnO nanoparticles reported good DPPH free radical scavenging activity compared to the reference standard ascorbic acid. The synthesized nanoparticles are biocompatible with human red blood cells and, hence, can be used to conjugate and deliver drugs due to increased biocompatibility at lower concentrations. The ZnO nanoparticles have significant potency against *C. quinquefasciatus* at 0.98 mg/L (LC_{50}) and 2.59 mg/L (LC_{90}), which asserts the ability of the nanoparticle to control insect vectors. Our research concludes that the above-mentioned green synthesized ZnO nanoparticle can be used as a potential therapeutic and nanodrug delivery system in the field of medicine and other fields as well. This study paves way for further in vivo, in vitro, animal model, and clinical trials to explore utility in biomedicine and pharmaceutical applications.

■ ASSOCIATED CONTENT

Data Availability Statement

All the data obtained are represented in tables, graphs, and figures.

Supporting Information

The Supporting Information is available free of charge at https://pubs.acs.org/doi/10.1021/acsomega.3c04857.

Diversified phytochemicals in *T. catappa* pericarp acting as stabilizers for NP synthesis; procedure for the synthesis of the ZnO nanoparticles using the fruit pericarp of *Terminalia catappa* Linn.; the particle size and other values interpreted using Debye−Scherrer's equation; mode of action of the synthesized ZnO nanoparticle on the cell wall of bacteria, mechanism of the synthesized ZnO nanoparticle exhibiting bacteriostatic activity, and mechanism of the synthesized ZnO nanoparticle exhibiting fungicidal activity; mechanism of the genotoxicity of synthesized ZnO nanoparticles on *Allium cepa* root tips; mode of action of the synthesized nanoparticles on human RBCs; and mode of action of the synthesized ZnO nanoparticle as a larvicide (PDF)

■ AUTHOR INFORMATION

Corresponding Author

Vasantha Veerappa Lakshmaiah − *Department of Life Sciences, CHRIST (Deemed to be University), Bangalore, Karnataka 560029, India;* orcid.org/0000-0001-7846-0304; Phone: 08040129717; Email: vasantha.vl@christuniversity.in

Authors

Cannon Antony Fernandes − *Department of Life Sciences, CHRIST (Deemed to be University), Bangalore, Karnataka 560029, India*

Nameeta Jesudoss M − *Department of Life Sciences, CHRIST (Deemed to be University), Bangalore, Karnataka 560029, India*

Aatika Nizam − *Department of Chemistry, CHRIST (Deemed to be University), Bangalore, Karnataka 560029, India*

Suresh Babu Naidu Krishna − *Department of Biomedical and Clinical Technology, Durban University of Technology,*

https://doi.org/10.1021/acsomega.3c04857
ACS Omega 2023, 8, 39315−39328

Durban 4000, South Africa; orcid.org/0000-0003-3155-8878

Complete contact information is available at: https://pubs.acs.org/10.1021/acsomega.3c04857

Author Contributions

All the authors had equally contributed toward the collection of data and interpretation.

Notes

The authors declare no competing financial interest.

■ ACKNOWLEDGMENTS

The authors are grateful to CHRIST (Deemed to be) University, Bengaluru; Xavier Research Foundation, Palayamkottai; Madurai Kamaraj University; Archbishop Casimir Instrumentation Centre, St.Joseph's College, Tiruchirappalli, for providing the research facilities. We are indebted to Dr. Delicia Avilla Barretto, Assistant Professor, School of Chemical Sciences, Goa University for her expert analysis on Antimicrobial and Antioxidant tests of the synthesized ZnO nanoparticles. Vasantha V L would like to thank CHRIST (Deemed to be University) for providing the support through the minor research project (MIRPDSC_1905).

■ REFERENCES

(1) Prasad, M.; Lambe, U. P.; Brar, B.; Shah, I.; J, M.; Ranjan, K.; Rao, R.; Kumar, S.; Mahant, S.; Khurana, S. K.; et al. Nanotherapeutics: An insight into healthcare and multi-dimensional applications in medical sector of the modern world. *Biomed. Pharmacother.* **2018**, *97*, 1521−1537.

(2) Singh, M.; Singh, S.; Prasad, S.; Gambhir, I. S. Nanotechnology, In Medicine And Antibacterial Effect Of Silver Nanoparticles. *Dig. J. Nanomater. Biostruct.* **2008**, *3*, 115.

(3) Radad, K.; Al-Shraim, M.; Moldzio, R.; Rausch, W.-D. Recent advances in benefits and hazards of engineered nanoparticles. *Environ. Toxicol. Pharmacol.* **2012**, *34* (3), 661−672.

(4) Maurer-Jones, M. A.; Gunsolus, I. L.; Murphy, C. J.; Haynes, C. L. Toxicity of Engineered Nanoparticles in the Environment. *Anal. Chem.* **2013**, *85* (6), 3036−3049.

(5) Nair, R.; Chanda, S. Antimicrobial activity of *Terminalia catappa, Manilkara zapota and Piper betel* leaf extract. *Indian J. Pharm. Sci.* **2008**, *70* (3), 390.

(6) Tigari, P.; Dupadahalli, K.; Kamurthy, H.; Nadendla, R.; Pandya, N. Antitumor and antioxidant status of Terminalia catappa against Ehrlich ascites carcinoma in Swiss albino mice. *Indian J. Pharmacol.* **2013**, *45* (5), 464.

(7) Terças, A. G.; Monteiro, A. d. S.; Moffa, E. B.; Santos, J. R. A. d.; Sousa, E. M. d.; Pinto, A. R. B.; Costa, P. C. d. S.; Borges, A. C. R.; Torres, L. M. B.; Barros Filho, A. K. D.; et al. Phytochemical Characterization of Terminalia catappa Linn. Extracts and Their antifungal Activities against Candida spp. *Front. Microbiol.* **2017**, *8*, 595.

(8) Ahmar Rauf, M..; Oves, M.; Ur Rehman, F.; Rauf Khan, A.; Husain, N. Bougainvillea flower extract mediated zinc oxide's nanomaterials for antimicrobial and anticancer activity. *Biomed. Pharmacother.* **2019**, *116*, 108983.

(9) NIAID Emerging Infectious Diseases/Pathogens. https://www.niaid.nih.gov/research/emerging-infectious-diseases-pathogens (accessed Sep 25, 2023)

(10) Oves, M.; Rauf, M. A.; Ansari, M. O.; Aslam Parwaz Khan, A.; A Qari, H.; Alajmi, M. F.; Sau, S.; Iyer, A. K. Graphene Decorated Zinc Oxide and Curcumin to Disinfect the Methicillin-Resistant Staphylococcus aureus. *Nanomaterials* **2020**, *10* (5), 1004.

(11) Aminuzzaman, M.; Ying, L. P.; Goh, W.-S.; Watanabe, A. Green synthesis of zinc oxide nanoparticles using aqueous extract of Garcinia mangostana fruit pericarp and their photocatalytic activity. *Bull. Mater. Sci.* **2018**, *41* (2), 50.

(12) Clinical and Laboratory Standards Institute. Performance Standards for Antimicrobial Disk Susceptibility Tests, Approved Standard, 7th ed. CLSI document M02-A11; Clinical and Laboratory Standards Institute: 950 West Valley Road, Suite 2500, Wayne, Pennsylvania 19087, USA. https://www.google.com/search?q=CLSI%2C+Performance+Standards+for+Antimicrobial+Disk+Susceptibility+Tests%2C+Approved+Standard%2C+7th+ed.%2C+CLSI+document+M02-A11.+Clinical+and+Laboratory+Standards+Institute%2C+950+West+Valley+Road%2C+Suite+2500%2C+Wayne%2C+Pennsylvania+19087%2C+USA%2C+2012a.+&rlz=1C1CHBF_enIN961IN961&sxsrf=AJOqlzWCQHEIiUGTGELFhGNo0y355Ye1Ng%3A1679157034592&ei=KucVZKDkI4eTseMPg6mqsAM&ved=0ahUKEwigoca08-X9AhWHSWwGHYOUCjYQ4dUDCA8&uact=5&oq=CLSI%2C+Performance+Standards+for+Antimicrobial+Disk+Susceptibility+Tests%2C+Approved+Standard%2C+7th+ed.%2C+CLSI+document+M02-A11.+Clinical+and+Laboratory+Standards+Institute%2C+950+West+Valley+Road%2C+Suite+2500%2C+Wayne%2C+Pennsylvania+19087%2C+USA%2C+2012a.+&gs_lcp=Cgxnd3Mtd2l6LXNlcnAQA0oECEEYAFAAWABgAGgAcAF4AIABAIgBAJIBAJgBAKABAqABAQ&sclient=gws-wiz-serp (accessed March 18, 2023).

(13) Clinical and Laboratory Standards Institute, Method for Antifungal Disk Diffusion Susceptibility Testing of Yeasts. Approved Guideline. CLSI document M44-A; Clinical and Laboratory Standards Institute: 940 West Valley Road, Suite 1400, Wayne, Pennsylvania 19087-1898, USA, 2004, https://www.google.com/search?q=CLSI%2C+Method+for+Antifungal+Disk+Diffusion+Susceptibility+Testing+of+Yeasts%2C+Approved+Guideline.+CLSI+document+M44-A.+CLSI%2C+940+West+Valley+Road%2C+Suite+1400%2C+Wayne%2C+Pennsylvania+19087-1898%2C+USA%2C+2004.&rlz=1C1CHBF_enIN961IN961&sxsrf=AJOqlzWh6wU6NbeMJOnmyC-EBBMi9JQV7Q%3A1679156964922&ei=5OYVZObrN_qUseMP-YiUuA0&ved=0ahUKEwjm7amT8-X9AhV6SmwGHXkEBdcQ4dUDCA8&uact=5&oq=CLSI%2C+Method+for+Antifungal+Disk+Diffusion+Susceptibility+Testing+of+Yeasts%2C+Approved+Guideline.+CLSI+document+M44-A.+CLSI%2C+940+West+Valley+Road%2C+Suite+1400%2C+Wayne%2C+Pennsylvania+19087-1898%2C+USA%2C+2004.&gs_lcp=Cgxnd3Mtd2l6LXNlcnAQA0oECEEYAFAAWABgAGgAcAF4AIABAIgBAJIBAJgBAKABAqABAQ&sclient=gws-wiz-serp (accessed March 18, 2023).

(14) Clinical and Laboratory Standards Institute. Methods for Dilution Antimicrobial Susceptibility Tests for Bacteria that Grow Aerobically, Approved Standard, 9th ed., CLSI document M07-A9; Clinical and Laboratory Standards Institute: 950 West Valley Road, Suite 2500, Wayne, Pennsylvania 19087, USA, 2012. https://www.google.com/search?q=CLSI%2C+Methods+for+Dilution+Antimicrobial+Susceptibility+Tests+for+Bacteria+that+Grow+Aerobically%2C+Approved+Standard%2C+9th+ed.%2C+CLSI+document+M07-A9.+Clinical+and+Laboratory+Standards+Institute%2C+950+West+Valley+Road%2C+Suite+2500%2C+Wayne%2C+Pennsylvania+19087%2C+USA%2C+2012b.&rlz=1C1CHBF_enIN961IN961&oq=CLSI%2C+Methods+for+Dilution+Antimicrobial+Susceptibility+Tests+for+Bacteria+that+Grow+Aerobically%2C+Approved+Standard%2C+9th+ed.%2C+CLSI+document+M07-A9.+Clinical+and+Laboratory+Standards+Institute%2C+950+West+Valley+Road%2C+Suite+2500%2C+Wayne%2C+Pennsylva

nia+19087%2C+USA%2C+2012b.&aqs=chrome..69i57.700j0j7&sourceid=chrome&ie=UTF-8 (accessed March 18, 2023).
(15) Brand-Williams, W.; Cuvelier, M. E.; Berset, C. Use of a free radical method to evaluate antioxidant activity. *LWT−Food Sci. Technol.* **1995**, *28* (1), 25−30.
(16) Hemanth Kumar, N. K.; Murali, M.; Satish, A.; Brijesh Singh, S.; Gowtham, H. G.; Mahesh, H. M.; Lakshmeesha, T. R.; Amruthesh, K. N.; Jagannath, S. Bioactive and Biocompatible Nature of Green Synthesized Zinc Oxide Nanoparticles from Simarouba glauca DC.: An Endemic Plant to Western Ghats, India. *J. Cluster Sci.* **2020**, *31* (2), 523−534.
(17) Sabir, S.; Arshad, M.; Chaudhari, S. K. Zinc Oxide Nanoparticles for Revolutionizing Agriculture: Synthesis and Applications. *Sci. World J.* **2014**, *2014*, 1−8.
(18) Murali, M.; Anandan, S.; Ansari, M. A.; Alzohairy, M. A.; Alomary, M. N.; Asiri, S. M. M.; Almatroudi, A.; Thriveni, M. C.; Singh, S. B.; Gowtham, H. G.; et al. Genotoxic and Cytotoxic Properties of Zinc Oxide Nanoparticles Phyto-Fabricated from the Obscure Morning Glory Plant Ipomoea obscura (L.) Ker Gawl. *Molecules* **2021**, *26* (4), 891.
(19) Nasar, M. Q.; Khalil, A. T.; Ali, M.; Shah, M.; Ayaz, M.; Shinwari, Z. K. Phytochemical Analysis, Ephedra Procera C. A. Mey. Mediated Green Synthesis of Silver Nanoparticles, Their Cytotoxic and Antimicrobial Potentials. *Medicina* **2019**, *55* (7), 369.
(20) Vijayakumar, S.; Vinoj, G.; Malaikozhundan, B.; Shanthi, S.; Vaseeharan, B. Plectranthus amboinicus leaf extract mediated synthesis of zinc oxide nanoparticles and its control of methicillin resistant Staphylococcus aureus biofilm and blood sucking mosquito larvae. *Spectrochim. Acta, Part A* **2015**, *137*, 886−891.
(21) World Health Organization *Report of the WHO Informal Consultation on the "Evaluation and Testing of Insecticides*: WHO/HQ, Geneva, 1996; 7 to 11 October 1996. https://apps.who.int/iris/bitstream/handle/10665/65962/CTD_WHOPES_IC_96.1.pdf.
(22) Yazhiniprabha, M.; Vaseeharan, B.; Sonawane, A.; Behera, A. In vitro and In vivo toxicity assessment of phytofabricated ZnO nanoparticles showing bacteriostatic effect and larvicidal efficacy against Culex quinquefasciatus. *J. Photochem. Photobiol., B* **2019**, *192*, 158−169.
(23) Pai, S.; Sridevi, S.; Varadavenkatesan, T.; Vinayagam, R.; Selvaraj, R. Photocatalytic zinc oxide nanoparticles synthesis using Peltophorum pterocarpum leaf extract and their characterization. *Optik* **2019**, *185*, 248−255.
(24) Barzinjy, A. A.; Azeez, H. H. Green synthesis and characterization of zinc oxide nanoparticles using Eucalyptus globulus Labill. leaf extract and zinc nitrate hexahydrate salt. *SN Appl. Sci.* **2020**, *2* (5), 991.
(25) Modena, M. M.; Rühle, B.; Burg, T. P.; Wuttke, S. Nanoparticle Characterization: What to Measure? *Adv. Mater.* **2019**, *31* (32), 1901556.
(26) Vimala, K.; Sundarraj, S.; Paulpandi, M.; Vengatesan, S.; Kannan, S. Green synthesized doxorubicin loaded zinc oxide nanoparticles regulates the Bax and Bcl-2 expression in breast and colon carcinoma. *Process Biochem.* **2014**, *49* (1), 160−172.
(27) Vishwajeet, S.; Ankita, S.; Nitin, W. Biosynthesis of silver nanoparticles by plants crude extracts and their characterization using UV, XRD, TEM and EDX. *Afr. J. Biotechnol.* **2015**, *14* (33), 2554−2567.
(28) Karimzadeh, M. R.; Soltanian, S.; Sheikhbahaei, M.; Mohamadi, N. Characterization and biological activities of synthesized zinc oxide nanoparticles using the extract of Acantholimon serotinum. *Green Process. Synth.* **2020**, *9* (1), 722−733.
(29) Degefa, A.; Bekele, B.; Jule, L. T.; Fikadu, B.; Ramaswamy, S.; Dwarampudi, L. P.; Nagaprasad, N.; Ramaswamy, K. Green Synthesis, Characterization of Zinc Oxide Nanoparticles, and Examination of Properties for Dye-Sensitive Solar Cells Using Various Vegetable Extracts. *J. Nanomater.* **2021**, *2021*, 1−9.
(30) Sarkar, S.; Sarkar, R. Synthesis, characterization and tribological study of zinc oxide nanoparticles. *Mater. Today: Proc.* **2021**, *44*, 3606−3612.
(31) Rajiv, P.; Rajeshwari, S.; Venckatesh, R. Bio-Fabrication of zinc oxide nanoparticles using leaf extract of Parthenium hysterophorus L. and its size-dependent antifungal activity against plant fungal pathogens. *Spectrochim. Acta, Part A* **2013**, *112*, 384−387.
(32) Faisal, S.; Jan, H.; Shah, S. A.; Shah, S.; Khan, A.; Akbar, M. T.; Rizwan, M.; Jan, F.; Wajidullah; Akhtar, N.; et al. Green Synthesis of Zinc Oxide (ZnO) Nanoparticles Using Aqueous Fruit Extracts of *Myristica fragrans*: Their Characterizations and Biological and Environmental Applications. *ACS Omega* **2021**, *6* (14), 9709−9722.
(33) Lakshmi, Y. V. B.; et al. Morphology and Anti-microbial Studies of Zinc Stannate Nanoparticles Constructed via Green Synthesis Approach. *Lett. Appl. NanoBioScience* **2022**, *12* (4), 138.
(34) Faruruwa, M., Awe, F., 2021. Green Synthesis, Characterization and Antibacterial Activity of Zinc Oxide and Titanium Dioxide Nanoparticles Using Terminalia Catappa and Cymbopogon Citratus. https://journalcps.com/index.php/volumes/article/view/302 (accessed Feb 22, 2023)
(35) Gudkov, S. V.; Burmistrov, D. E.; Serov, D. A.; Rebezov, M. B.; Semenova, A. A.; Lisitsyn, A. B. A Mini Review of Antibacterial Properties of ZnO Nanoparticles. *Front. Phys.* **2021**, *9*, 641481.
(36) Akbar, A.; Sadiq, M. B.; Ali, I.; Muhammad, N.; Rehman, Z.; Khan, M. N.; Muhammad, J.; Khan, S. A.; Rehman, F. U.; Anal, A. K. Synthesis and antimicrobial activity of zinc oxide nanoparticles against foodborne pathogens Salmonella typhimurium and Staphylococcus aureus. *Biocatal. Agric. Biotechnol.* **2019**, *17*, 36−42.
(37) Janaki, A. C.; Sailatha, E.; Gunasekaran, S. Synthesis, characteristics and antimicrobial activity of ZnO nanoparticles. *Spectrochim. Acta, Part A* **2015**, *144*, 17−22.
(38) Yusof, N. A. A.; Zain, N. M.; Pauzi, N. Synthesis of ZnO nanoparticles with chitosan as stabilizing agent and their antibacterial properties against Gram-positive and Gram-negative bacteria. *Int. J. Biol. Macromol.* **2019**, *124*, 1132−1136.
(39) Kashef, N.; Huang, Y.-Y.; Hamblin, M. R. Advances in antimicrobial photodynamic inactivation at the nanoscale. *Nanophotonics* **2017**, *6* (5), 853−879.
(40) Padalia, H.; Moteriya, P.; Khara, G.; Chanda, S. WITHDRAWN: Green synthesis, characterization, antimicrobial and cytotoxic activities of zinc oxide nanoparticles from Cinnamomum verum bark extract. *OpenNano* **2017**.
(41) Murali, M.; Kalegowda, N.; Gowtham, H. G.; Ansari, M. A.; Alomary, M. N.; Alghamdi, S.; Shilpa, N.; Singh, S. B.; Thriveni, M. C.; Aiyaz, M.; et al. Plant-Mediated Zinc Oxide Nanoparticles: Advances in the New Millennium towards Understanding Their Therapeutic Role in Biomedical Applications,. *Pharmaceutics* **2021**, *13* (10), 1662.
(42) Sharmila, G.; Muthukumaran, C.; Sandiya, K.; Santhiya, S.; Pradeep, R. S.; Kumar, N. M.; Suriyanarayanan, N.; Thirumarimurugan, M. Biosynthesis, characterization, and antibacterial activity of zinc oxide nanoparticles derived from Bauhinia tomentosa leaf extract. *J. Nanostruct. Chem.* **2018**, *8* (3), 293−299.
(43) Iyer, K. R.; Robbins, N.; Cowen, L. E. The role of Candida albicans stress response pathways in antifungal tolerance and resistance. *iScience* **2022**, *25* (3), 103953.
(44) Vijayakumar, S.; Vidhya, E.; Nilavukkarasi, M.; Punitha, V. N.; Praseetha, P. K. Potential eco-friendly Zinc Oxide nanomaterials through Phyco-nanotechnology -A review. *Biocatal. Agric. Biotechnol.* **2021**, *35*, 102050.
(45) Djearamane, S.; Xiu, L. J.; Wong, L. S.; Rajamani, R.; Bharathi, D.; Kayarohanam, S.; De Cruz, A. E.; Tey, L. H.; Janakiraman, A. K.; Aminuzzaman, M.; et al. Antifungal Properties of Zinc Oxide Nanoparticles on Candida albicans. *Coatings* **2022**, *12* (12), 1864.
(46) Gow, N. A. R.; Latge, J.-P.; Munro, C. A., The Fungal Cell Wall: Structure, Biosynthesis, and Function *Microbiol. Spectrum*, *5*,3, **2017**, .
(47) Nagajyothi, P. C.; Cha, S. J.; Yang, I. J.; Sreekanth, T. V. M.; Kim, K. J.; Shin, H. M. Antioxidant and anti-inflammatory activities of zinc oxide nanoparticles synthesized using Polygala tenuifolia root extract. *J. Photochem. Photobiol., B* **2015**, *146*, 10−17.

https://doi.org/10.1021/acsomega.3c04857
ACS Omega 2023, 8, 39315−39328

(48) Siripireddy, B.; Mandal, B. K. Facile green synthesis of zinc oxide nanoparticles by Eucalyptus globulus and their photocatalytic and antioxidant activity. *Adv. Powder Technol.* **2017**, *28* (3), 785−797.
(49) Sowmya, T. N.; Raveesha, K. A. Polyphenol-Rich Purified Bioactive Fraction Isolated from Terminalia catappa L.: UHPLC-MS/MS-Based Metabolite Identification and Evaluation of Their Antimicrobial Potential. *Coatings* **2021**, *11* (10), 1210.
(50) Sirelkhatim, A.; Mahmud, S.; Seeni, A.; Kaus, N. H. M.; Ann, L. C.; Bakhori, S. K. M.; Hasan, H.; Mohamad, D. Review on Zinc Oxide Nanoparticles: Antibacterial Activity and Toxicity Mechanism. *Nano-Micro Lett.* **2015**, *7* (3), 219−242.
(51) Mahendra, C.; Murali, M.; Manasa, G.; Ponnamma, P.; Abhilash, M.; Lakshmeesha, T.; Satish, A.; Amruthesh, K.; Sudarshana, M. Antibacterial and antimitotic potential of bio-fabricated zinc oxide nanoparticles of Cochlospermum religiosum (L.). *Microb. Pathog.* **2017**, *110*, 620−629.
(52) Asita, A. O.; Mokhobo, M. Clastogenic and Cytotoxic Effects of Four Pesticides Used to Control Insect Pests of Stored Products on Root Meristems of Allium cepa. *Environ. Nat. Resour. Res.* **2013**, *3* (2), 133.
(53) Fadoju, O. M.; Osinowo, O. A.; Ogunsuyi, O. I.; Oyeyemi, I. T.; Alabi, O. A.; Alimba, C. G.; Bakare, A. A. Interaction of titanium dioxide and zinc oxide nanoparticles induced cytogenotoxicity in Allium cepa. *Nucleus* **2020**, *63* (2), 159−166.
(54) Kumar, D.; Rajeshwari, A.; Jadon, P. S.; Chaudhuri, G.; Mukherjee, A.; Chandrasekaran, N.; Mukherjee, A. Cytogenetic studies of chromium (III) oxide nanoparticles on Allium cepa root tip cells. *J. Environ. Sci.* **2015**, *38*, 150−157.
(55) Sun, Z.; Xiong, T.; Zhang, T.; Wang, N.; Chen, D.; Li, S. Influences of zinc oxide nanoparticles on Allium cepa root cells and the primary cause of phytotoxicity. *Ecotoxicology* **2019**, *28* (2), 175−188.
(56) Saboo, S. S.; Tapadiya, G. G.; Lamale, J. J.; Khadabadi, S. S. Phytochemical screening and antioxidant, antimitotic, and antiproliferative activities of Trichodesma indicum shoot. *Anc. Sci. Life* **2014**, *34* (2), 113−118.
(57) Taranath, T. C.; Patil, B. N.; Santosh, T. U.; Sharath, B. S. Cytotoxicity of zinc nanoparticles fabricated by Justicia adhatoda L. on root tips of Allium cepa L.—a model approach. *Environ. Sci. Pollut. Res.* **2015**, *22* (11), 8611−8617.
(58) Tettey, C. O.; Shin, H. M. Evaluation of the antioxidant and cytotoxic activities of zinc oxide nanoparticles synthesized using scutellaria baicalensis root. *Sci. Afr.* **2019**, *6*, No. e00157.
(59) Dietz, K.-J.; Herth, S. Plant nanotoxicology. *Trends Plant Sci.* **2011**, *16* (11), 582−589.
(60) Mousavi Kouhi, S. M.; Lahouti, M.; Ganjeali, A.; Entezari, M. H. Comparative phytotoxicity of ZnO nanoparticles, ZnO microparticles, and Zn^{2+} on rapeseed (*Brassica napus* L.): investigating a wide range of concentrations. *Toxicol. Environ. Chem.* **2014**, *96* (6), 861−868.
(61) Ahmed, B.; Dwivedi, S.; Abdin, M. Z.; Azam, A.; Al-Shaeri, M.; Khan, M. S.; Saquib, Q.; Al-Khedhairy, A. A.; Musarrat, J. Mitochondrial and Chromosomal Damage Induced by Oxidative Stress in Zn2+ Ions, ZnO-Bulk and ZnO-NPs treated Allium cepa roots. *Sci. Rep.* **2017**, *7* (1), 40685.
(62) El-Khodary, S.; Habib, A.; Haliem, A. Effects of the herbicide Tribunil on root mitosis of Allium cepa. *Cytologia* **1990**, *55* (2), 209−215.
(63) El-Khodary, S.; Habib, A.; Haliem, A. Cytological effect of the herbicide Garlon-4 on root mitosis of Allium cepa. *Cytologia* **1989**, *54* (3), 465−472.
(64) Kumari, M.; Khan, S. S.; Pakrashi, S.; Mukherjee, A.; Chandrasekaran, N. Cytogenetic and genotoxic effects of zinc oxide nanoparticles on root cells of Allium cepa. *J. Hazard. Mater.* **2011**, *190* (1−3), 613−621.
(65) Badawy, A. A.; Abdelfattah, N. A. H.; Salem, S. S.; Awad, M. F.; Fouda, A. Efficacy Assessment of Biosynthesized Copper Oxide Nanoparticles (CuO-NPs) on Stored Grain Insects and Their Impacts on Morphological and Physiological Traits of Wheat (Triticum aestivum L.) Plant. *Biology* **2021**, *10* (3), 233.
(66) Gunathilaka, U. M. T. M.; de Silva, W. A. P. P.; Dunuweera, S. P.; Rajapakse, R. M. G. Effect of morphology on larvicidal activity of chemically synthesized zinc oxide nanoparticles against mosquito vectors. *RSC Adv.* **2021**, *11* (15), 8857−8866.
(67) Abdo, A. M.; Fouda, A.; Eid, A. M.; Fahmy, N. M.; Elsayed, A. M.; Khalil, A. M. A.; Alzahrani, O. M.; Ahmed, A. F.; Soliman, A. M. Green Synthesis of Zinc Oxide Nanoparticles (ZnO-NPs) by Pseudomonas aeruginosa and Their Activity against Pathogenic Microbes and Common House Mosquito, Culex pipiens. *Materials* **2021**, *14* (22), 6983.
(68) Fouda, A.; Awad, M. A.; Eid, A. M.; Saied, E.; Barghoth, M. G.; Hamza, M. F.; Awad, M. F.; Abdelbary, S.; Hassan, S. E. D. An Eco-Friendly Approach to the Control of Pathogenic Microbes and Anopheles stephensi Malarial Vector Using Magnesium Oxide Nanoparticles (Mg-NPs) Fabricated by Penicillium chrysogenum. *Int. J. Mol. Sci.* **2021**, *22* (10), 5096.
(69) Benelli, G. Mode of action of nanoparticles against insects. *Environ. Sci. Pollut. Res.* **2018**, *25* (13), 12329−12341.
(70) Achudhan, D.; Vijayakumar, S.; Malaikozhundan, B.; Divya, M.; Jothirajan, M.; Subbian, K.; González-Sánchez, Z. I.; Mahboob, S.; Al-Ghanim, K. A.; Vaseeharan, B. The antibacterial, antibiofilm, antifogging and mosquitocidal activities of titanium dioxide (TiO2) nanoparticles green-synthesized using multiple plants extracts. *J. Environ. Chem. Eng.* **2020**, *8* (6), 104521.
(71) Al-Dhabi, N.; Valan Arasu, M. Environmentally-Friendly Green Approach for the Production of Zinc Oxide Nanoparticles and Their Anti-Fungal, Ovicidal, and Larvicidal Properties. *Nanomaterials* **2018**, *8* (7), 500.

https://doi.org/10.1021/acsomega.3c04857
ACS Omega 2023, 8, 39315−39328